

# Effect of Co Substitution on Ferrimagnetic Heusler compound $\text{Mn}_3\text{Ga}$

Quynh Anh T. Nguyen<sup>1</sup>, Thi H. Ho<sup>1</sup>, Myung-Hwa Jung<sup>2</sup>, and Sonny H. Rhim<sup>1\*</sup>

<sup>1</sup>*Department of Physics and Energy Harvest Storage Research Center, University of Ulsan, Ulsan 44610, Republic of Korea*

<sup>2</sup>*Department of Physics, Sogang University, Seoul, 04107, Republic of Korea*

(Dated: September 22, 2022)

Effect of Co substitution on  $\text{Mn}_3\text{Ga}$  is investigated using first-principles study for structural and magnetic properties. Without Co, ferrimagnetic Heusler compound  $\text{Mn}_3\text{Ga}$  is in tetragonal phase. With Co substitution, depending on Co concentration ( $x$ )  $\text{Mn}_3\text{Ga}$  prefers tetragonal (cubic) phase when  $x \leq 0.5$  ( $x \geq 0.5$ ). Ferrimagnetism is robust regardless of  $x$  in both phases. While magnetic moments of two Mn do not vary significantly with  $x$ , Co magnetic moment in two phases exhibit different behaviors, leading to distinct features in total magnetic moment ( $M_{\text{tot}}$ ). When  $x \leq 0.5$ , in tetragonal phase, Co magnetic moment is vanishingly small, resulting in a decrease of  $M_{\text{tot}}$  with  $x$ . In contrast, when  $x \geq 0.5$ , in cubic phase, Co magnetic moment is roughly  $1\mu_B$ , which is responsible for an increase of  $M_{\text{tot}}$ . Electronic structure is analyzed with partial density of states for various  $x$ . To elucidate the counterintuitively small Co moment, the magnetic exchange interaction is investigated where exchange coefficient between Co and Mn is much smaller in  $x \leq 0.5$  case than  $x \geq 0.5$  one.

## I. Introduction

For decades, Heusler compounds with plethora of material classes have drawn continuously renewed attentions [1, 2]. Rich physics has been platforms for various research. Numerous functionalities and properties, such as superconductivity, magnetism, multiferroicity, half-metallicity, topological insulators, and so forth [3–6], have attracted for applications in many areas. In particular, in the context of rapid progress in magnetic devices and spintronics, tetragonal Heusler compounds have been intensively and extensively explored. Properties of tetragonal Heusler compounds, perpendicular magnetic anisotropy (PMA) and low saturation magnetization ( $M_S$ ) [7–9], are regarded advantageous in applications with low switching current ( $I_S$ ) [10–12].

$\text{Mn}_3\text{Ga}$  belonging to Heusler family in tetragonal structure, possesses aforementioned magnetic properties: strong PMA around  $0.89 \text{ MJ/m}^{-3}$ , high Curie temperature ( $T_C$ ) of 740 K [13, 14], low  $M_S$  around  $200 \text{ emu/cm}^3$ , and approximately 58% of spin polarization [15]. Low  $M_S$  stems from the intrinsic ferrimagnetism of antiparallel alignment of two Mn moments with unequal magnitudes. Efforts have been devoted to enhance the magnetic properties of  $\text{Mn}_3\text{Ga}$ . One is to replace Mn by other transition metal (TM) [16] where V-shape magnetization with respect to TM content ( $x$ ) is quite distinct. Upon substitution of nonmagnetic TM,  $M_{\text{tot}}$  decreases with  $x$  as nonmagnetic TM replaces one Mn, moment is reduced but the antiparallel moment with the other Mn is retained.  $M_{\text{tot}} = 0$  is achieved for certain  $x$  above which the survived antiparallel moment dominates hence  $M_{\text{tot}}$  increases.

The V-shape of magnetization is also prominent with magnetic TM substitution such as Fe, Co, and Ni [17, 18]. However,  $M_{\text{tot}}$  nearly vanishes above  $x = 0.5$  and is not compensated. Interestingly, Co substitution accompanies a structural transition from tetragonal to cubic while the substitution by Fe and Ni retains the tetragonal structure. Moreover, the magnetic behavior of magnetic TM in two structural phases is different. Magnetic moments in tetragonal phase are smaller than

the bulk counterpart but those in cubic phase are comparable to the bulk ones. While the substitution of Fe results in hard magnet and that of Ni exhibits the shape memory phenomena, the property of Co substitution depends on the Co content. It has been reported earlier that Co-poor ( $0 < x < 0.5$ ) in tetragonal alloy is well suited for spin-transfer torque (STT) whereas Co-rich ( $0.5 < x < 1$ ) favors cubic phase with half-metallicity. As STT and half-metallicity are favorable components in spintronic application, further study would shed light on uncovering  $\text{Mn}_{3-x}\text{Co}_x\text{Ga}$ .

In this paper, employing *ab initio* calculations, the effect of Co substitution on  $\text{Mn}_{3-x}\text{Co}_x\text{Ga}$  is investigated. Magnetic property of  $\text{Mn}_{3-x}\text{Co}_x\text{Ga}$  is illustrated along with total as well as atomic resolved magnetic moments. Analysis follows to reveal the electronic structure of  $\text{Mn}_{3-x}\text{Co}_x\text{Ga}$ . To elucidate the contrasting behavior of Co magnetism in two phases, tetragonal and cubic, the exchange coefficients are discussed in the framework of the magnetic force theorem using the Heisenberg model.

## II. Structure and computational Methods

Tetragonal ( $x = 0$ ) and cubic phases ( $x = 1$ ) are presented in Fig. 1, which correspond to  $D0_{22}$  and  $L_{21}$  structure, respectively. Both tetragonal and cubic phase have two inequivalent Mn atoms distinguished by Mn(I) and Mn(II). Space group of tetragonal phase is  $I4/mmm$  (No. 139) and that of cubic phase is  $Fm\bar{3}m$  (No. 225). Wyckoff positions of both phases are listed in Table I.

TABLE I. Wyckoff positions of constituent atoms of tetragonal and cubic phases, whose space groups are  $I4/mmm$  (No.139) and  $Fm\bar{3}m$  (No.25), respectively. Co takes either  $2c$  or  $2d$  site.

	Tetragonal	Cubic
Mn(I)	$2b$	$4a$
Mn(II)	$4d$	$4c$
Ga	$2a$	$4b$
Co	$2c/2d$	$4d$

\* sonny@ulsan.ac.kr

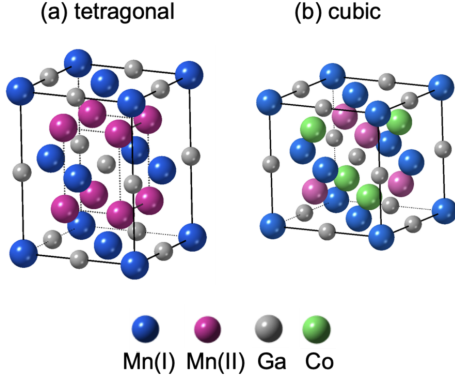


FIG. 1. Crystal structure of (a) tetragonal  $\text{Mn}_3\text{Ga}$  and (b) cubic  $\text{Mn}_2\text{CoGa}$ . Blue, red, green and grey spheres denote Mn(I), Mn(II), Co and Ga atoms, respectively.

First-principles calculations are performed using Vienna *Ab initio* Simulation Package (VASP) [19, 20] with projector augmented-wave basis [21]. The exchange-correlation potential is treated using generalized gradient approximation (GGA) with Perdew, Burke, and Ernzerhof (PBE) parametrization [22, 23]. Cutoff energy of 500 eV is employed for wave function expansion. For Brillouin zone integration,  $15 \times 15 \times 7$  and  $15 \times 15 \times 11$   $k$  meshes are used for tetragonal and cubic phases, respectively, where  $\sqrt{2}/2 \times \sqrt{2}/2 \times 1$  unit cell is adopted for the primitive cell.

From lattice constant optimization, we obtain  $a = 3.78$  Å ( $c/a = 1.88$ ) for tetragonal phase and  $a = 4.12$  Å for cubic phase, respectively, which are used for further calculations. The exchange coefficients are calculated using the Heisenberg model in the framework of the magnetic force theorem (MFT) [24]. To do so, additional self-consistent calculations are performed using OpenMX [25], where atomic basis sets for Mn, Ga, and Co are  $s3p2d1$ ,  $s2p2d1$ , and  $H-s3p2d1$ , respectively with energy cutoff of 300 Ry and cutoff radii of 10.0 Å (Mn and Co) and 9.0 Å (Ga), respectively. Then,  $Jx$  package is employed [26–28] to extract the exchange coefficients ( $J$ ) in the framework of MFT.

### III. Results and Discussion

#### A. Magnetic Moments

$\text{Mn}_3\text{Ga}$  is either tetragonal or cubic depending on Co concentration  $x$ . When  $x < 0.5$ , tetragonal phase with  $c/a = 1.88$  is favored whereas when  $x > 0.5$  cubic phase is preferred. As such,  $x = 0.5$  is a phase boundary of two phases [29].

Total magnetic moment ( $M_{\text{tot}}$ ) as function of  $x$  is plotted in Fig. 2, where each moment of individual Co, Mn(I), and Mn(II) is also shown. For all  $x$ ,  $\text{Mn}_{3-x}\text{Co}_x\text{Ga}$  is ferrimagnetic: Moments of Mn(I) and Mn(II) are antiparallel with different magnitudes. Without Co, i.e.  $x = 0$ , Mn(I) and Mn(II) have moments of  $2.87$  and  $-2.32 \mu_B$ , respectively, exhibiting indeed ferrimagnetism. Total magnetic moment ( $M_{\text{tot}}$ ) is  $1.72 \mu_B$  per

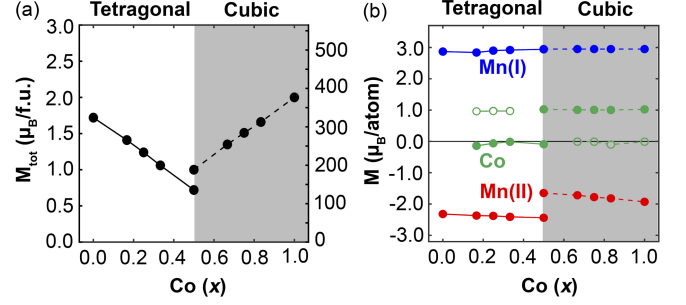


FIG. 2. (a) Magnetic moment ( $M_{\text{tot}}$ ) per unit cell with respect to  $x$ , where white and grey area are tetragonal and cubic phases, respectively. Right axis is in  $\text{emu}/\text{cm}^3$  converted from  $\mu_B$  on the left axis. (b) Atom-resolved magnetic moment: blue, red, and green circles denote Mn(I), Mn(II), and Co, respectively. Open (solid) circles represent unstable (stable) phase.

formula unit, consistent with previous works [14, 30], which corresponds to magnetization of  $314 \text{ emu}/\text{cm}^3$ . As shown in Fig. 2(a),  $M_{\text{tot}}$  decreases (increases) with  $x$  in tetragonal (cubic) phase. Notably, at the phase boundary when  $x = 0.5$ ,  $M_{\text{tot}}$  of cubic phase is larger by  $0.4 \mu_B$  than tetragonal phase. This difference is due to different Co magnetism in both phases. Acknowledging ferromagnetism of Co, Co moment in tetragonal phase is quite small [31], which is against to the conventional wisdom. This is discussed later in Sec. III B and III C.

Magnetic moments of individual atoms are shown in Fig. 2(b) [32]. For all  $x$ , Mn(I) and Mn(II) have almost constant moments with  $2.90$  and  $-2.32 \mu_B$ , respectively. However, Co moment in tetragonal phase nearly vanishes while in cubic phase is around  $1.0 \mu_B$ . Consequently,  $M_{\text{tot}}$  decreases with  $x$  in tetragonal phase:  $M_{\text{tot}} = 1.72 \mu_B$  for  $x = 0$  drops to  $0.72 \mu_B$  for  $x = 0.5$ . On the other hand, in cubic phase, more Co substitution results in increase of  $M_{\text{tot}}$  from  $1.00$  to  $2.00 \mu_B$ . The vanishingly small Co magnetic moment in tetragonal phase is also reported in previous work which has been also reported in other theoretical work [33]. As mentioned earlier, this counterintuitive feature will be visited in III C.

#### B. Electronic Structure

Partial density of states (PDOS) is presented in Fig. 3. Left (right) upper panel is tetragonal (cubic) phase for  $x = 0$  ( $x = 1$ ). Lower panel is for  $x = 0.5$  of tetragonal and cubic phases, respectively. Important peaks are labelled with triangle marks: 1, 2, and C stand for Mn(I), Mn(II), and Co, respectively; + (-) for the majority (minority) spin state, respectively. Different peaks in the same spin state of particular atom are distinguished by primes. PDOS's of  $x = 1/3$  and  $2/3$  are shown in Fig. S3, where the vertical line serves to manifest the overall trend upon  $x$ . The shift of  $E_F$  by Co substitution is evidence as Co has two more electrons than Mn [34].

In tetragonal phase with  $x = 0$  [Fig. 3(a)], Mn(I) and Mn(II) exhibit distinct features. Mn(I) has two main peaks: 1+ (1-) in occupied (empty) states around  $-2.7$  eV ( $+1.0$  eV) in the

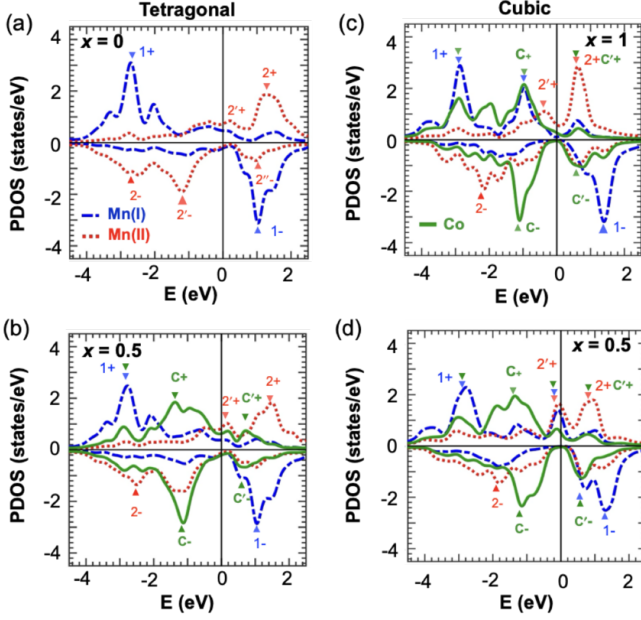


FIG. 3. Partial density of states (PDOS) of  $d$  orbitals. Left and right panels for tetragonal and cubic phases, respectively. Tetragonal phase with (a)  $x = 0$  and (b)  $x = 0.5$ . Cubic phase with (c)  $x = 1.0$  and (d)  $x = 0.5$ . Lower panel is comparison between tetragonal and cubic phases with  $x = 0.5$ . Blue, red, and green lines denote  $d$  orbitals of Mn(I), Mn(II), and Co, respectively. Peaks are emphasized with triangles. Fermi energy ( $E_F$ ) is set to zero.

majority (minority) spin state. On the other hand, Mn(II) has rather broader peak with smaller height than Mn(I):  $2+$  around  $+1.3$  eV in the majority spin state and  $2-$ ,  $2'-$ , and  $2''-$  around  $-2.5$ ,  $-1.2$  eV, and  $+1.0$  eV in the minority spin state, respectively.

For  $x = 0.5$  in tetragonal phase [Fig. 3(b)], Mn(I) and Mn(II) PDOS do not change much with respect to  $x = 0$  but shifted by  $+0.20$  eV due to Co. [See vertical line in Fig. S3]. On the other hand, several peaks emerge in Co PDOS. As Co replaces Mn(II), most Co peaks overlap with Mn(II):  $C-$  coincides with  $2'-$  and small hump just above  $E_F$  overlap with  $2'+$ . Nonetheless, the overlap with Mn(I) in the majority spin state around  $-2.8$  eV (marked with double triangles) is evident. Broad  $C+$  appear between  $-1.4$  and  $0.4$  eV owing to hybridization with Ga  $p$  state [See Fig. S2]. In particular, there are small humps around  $+0.2$  and  $+0.6$  eV, where the former, just mentioned earlier, overlaps with  $2'+$  but the latter has no such feature. As the sum of occupied PDOS of two spin states is almost equal, Co magnetic moment nearly vanishes, which is prominent in tetragonal phase.

Now we switch to cubic phase with  $x = 1$  [Fig. 3(c)]. Compared to  $x = 0$  of tetragonal phase,  $1+$  changes little but  $1-$  shifts by  $+0.3$  eV. However, changes in Mn(II) and Co are apparent. In the minority spin state,  $2-$  shifts by  $0.2$  eV and  $2'-$  is replaced by  $C-$ . Overlaps between  $2''-$  (not labeled) and  $C'-$  are prominent around  $E_F + 0.8$  eV. On the other hand, in the majority spin state,  $C+$  appears almost around the same place as  $C-$ . Overlaps between  $C'+$  and  $2+$  around  $E_F + 0.6$  eV are

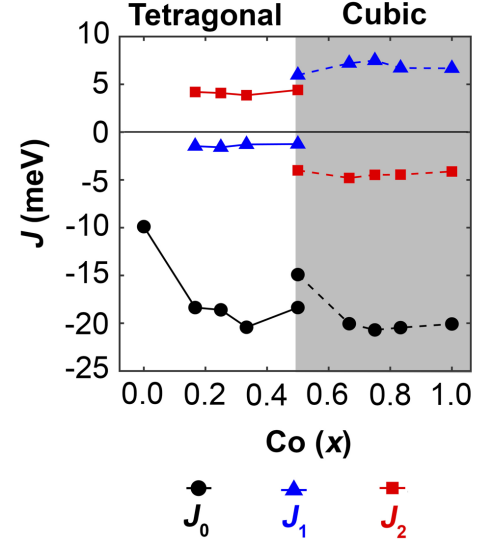


FIG. 4. Calculated exchange coefficients ( $J$ ) for nearest neighbor interactions for various  $x$  ( $0 \leq x \leq 1$ ).  $J_0$ ,  $J_1$ , and  $J_2$ , represent the exchange coefficients of Mn(I)-Mn(II), Co-Mn(I), Co-Mn(II) in black, blue, and red, respectively. Tetragonal and cubic regions are divided by white and grey regions. Solid and dashed lines for tetragonal and cubic phases, respectively.

much closer to  $E_F$  than  $x = 0$ . Notably,  $2'+$  is occupied in contrast to  $x = 0$ .

Cubic phase with  $x = 0.5$  is shown in Fig. 3(d). Here, we discuss changes with respect to  $x = 0.5$  of tetragonal phase and  $x = 1$  of cubic phase. Hence in this paragraphs  $x = 0.5$  ( $x = 1.0$ ) refers to that in tetragonal (cubic) phase. Mn(I) is little affected:  $1+$  and  $1-$  change negligibly with respect to  $x = 1$  whereas  $1-$  shifts by  $+0.3$  eV with respect to  $x = 0.5$ . On the other hand, Mn(II) is quite affected with negative (positive) shifts with respect to  $x = 0.5$  ( $x = 1$ ). More specifically, compared to  $x = 1$ , peaks of  $2+$  and  $2'+$  shift by  $+0.30$  and  $+0.20$  eV, respectively; that of  $2-$  by  $+0.35$  eV. Compared to  $x = 0.5$ , shifts of  $2+$  and  $2'+$  are  $-0.60$  and  $-0.40$  eV, respectively;  $2-$  by  $-0.50$  eV. In particular,  $2'+$  accompanies occupation change. For Co PDOS,  $C+$  and  $C-$  shift by  $-0.4$  and  $-0.1$  eV, respectively, with respect to  $x = 1$ , and  $0$  and  $-0.1$  eV with respect to  $x = 0.5$ . Positive shift of Mn(II) with respect to  $x = 1$  is well expected, as mentioned earlier, as Co has more electrons than Mn.

### C. Magnetic Exchange Interaction

So far PDOS analysis is presented. While Co magnetic moment in cubic phase ( $x \geq 0.5$ ) is around  $1 \mu_B$ , that in tetragonal phase  $x \leq 0.5$  nearly vanishes, which is against the conventional wisdom. In order to clarify this puzzling Co magnetism, the exchange coefficients,  $J$ , are discussed, employing the Heisenberg model,  $\hat{H} = -\sum_{ij} J_{ij} \mathbf{S}_i \cdot \mathbf{S}_j$ , where  $J_{ij}$ , the exchange coefficients, with positive (negative) sign implies parallel (antiparallel) magnetic coupling. As briefly mentioned

in II,  $J$ 's are calculated in the framework of MFT [24–26, 28]. Fig.4 shows calculations of the exchange coefficients for three cases, Mn(I)-Mn(II), Co-Mn(I), and Co-Mn(II), denoted as  $J_0$ ,  $J_1$ , and  $J_2$ , respectively.

$J_0$ , the exchange coefficients for two Mn types, is negative for all cases. This indicates the antiparallel magnetism between two Mn sites confirming the ferrimagnetism. Moreover,  $|J_0|$  is larger than  $|J_1|$  or  $|J_2|$  roughly by an order of magnitude. In tetragonal phase ( $x \leq 0.5$ ),  $J_0 = -9.89$  meV for  $x = 0$  whose magnitude increases with  $x$  ranging 18 – 21 meV. In cubic phase ( $x \geq 0.5$ ),  $J_0 = -14.9$  meV for  $x = 0.5$ , whose magnitude also increases with  $x$  up to 20 meV. From this, addition of Co introduces stronger tendency of the antiparallel magnetism between Mn(I) and Mn(II).

The exchange coefficients between Co-Mn(I) and Co-Mn(II), namely  $J_1$  and  $J_2$ , exhibit opposite sign behavior where magnitudes in cubic phase are slightly larger. In contrast to  $J_0$ , both  $|J_1|$  and  $|J_2|$  are little influenced by Co. In tetragonal phase,  $|J_1|$  and  $|J_2|$  are approximately 1 and 5 meV, respectively, while in cubic phase  $|J_1|$  and  $|J_2|$  are approximately 5 and 7 meV, respectively. The opposite signs of  $J_1$  and  $J_2$  is due to the antiparallel magnetism between Mn(I) and Mn(II). From  $|J_2| > |J_1|$ , the antiparallel coupling between Co-Mn(II) is stronger than Co-Mn(I). Moreover,  $J_1$  and  $J_2$  change signs between tetragonal and cubic phases, henceforth Co shows the opposite sign of magnetic moment in both phases. From the analysis of the exchange coefficients, Mn(I) and Mn(II) exhibit rather rigid magnetic moments. Moreover, the exchange coefficients with Co in tetragonal phase are weaker than cubic phase. As a result, Co moments in tetrago-

nal phase is smaller than cubic one.

#### IV. Conclusion

In summary, we have investigated the effect of Co substitution on  $\text{Mn}_3\text{Ga}$  for structural and magnetic properties. The ferrimagnetic feature is robust regardless of Co concentration ( $x$ ). When  $x \leq 0.5$ , tetragonal phase is favored over cubic and vice versa, where the magnetic behavior of each phase is different. In tetragonal phase,  $M_{\text{tot}}$  decreases with  $x$  while in cubic phase  $M_{\text{tot}}$  increases with  $x$ . Electronic structure upon Co substitution is investigated with PDOS, whose peak structures are analyzed. Except Co, magnetic moments of individual atom change little with  $x$ . Co magnetic moment in tetragonal phase nearly vanishes in contrast to  $1\mu_B$  of cubic phase. To get more insight on this contrasting Co moment in two phases, the exchange coefficients are estimated using the Heisenberg model. Indeed, the antiparallel magnetism, more precisely, the ferrimagnetism between Mn(I)-Mn(II) with different magnitudes is well manifested. On the other hand, the exchange coefficients of Co-Mn(I) and Co-Mn(II) exhibit opposite signs in tetragonal and cubic phase.

#### Acknowledgments

We are grateful to Soon Cheol Hong for fruitful discussions and comments. This work was supported by the National Research Foundation (NRF) of Korea (2019R1I1A3A01059880, 2020R1A2C3008044).

- 
- [1] K. Manna, Y. Sun, L. Muechler, J. Kübler, and C. Felser, Heusler, Weyl, and Berry, *Nat. Rev. Mater.* **3**, 244 (2018).
  - [2] L. Wollmann, A. K. Nayak, S. S. Parkin, and C. Felser, Heusler 4.0: tunable materials, *Annu. Rev. Mater. Res.* **47**, 247 (2017).
  - [3] Y. Kurtulus, R. Dronskowski, G. D. Samolyuk, and V. P. Antropov, Electronic structure and magnetic exchange coupling in ferromagnetic full Heusler alloys, *Phys. Rev. B* **71**, 014425 (2005).
  - [4] T. Graf, C. Felser, and S. S. P. Parkin, Simple rules for the understanding of Heusler compounds, *Prog. Solid State Chem.* **39**, 1 (2011).
  - [5] M. Sargolzaei, M. Richter, K. Koepernik, I. Opahle, H. Eschrig, and I. Chaplygin, Spin and orbital magnetism in full Heusler alloys: A density functional theory study of  $\text{Co}_2\text{YZ}$  ( $\text{Y} = \text{Mn}, \text{Fe}$ ;  $\text{Z} = \text{Al}, \text{Si}, \text{Ga}, \text{Ge}$ ), *Phys. Rev. B* **74**, 224410 (2006).
  - [6] S. Ishida, S. Fujii, S. Kashiwagi, and S. Asano, Search for half-metallic compounds in  $\text{Co}_2\text{MnZ}$  ( $\text{Z} = \text{IIIb}, \text{IVb}, \text{Vb}$  element), *J. Phys. Soc. Jpn.* **64**, 2152 (1995).
  - [7] T. Gasi, A. K. Nayak, J. Winterlik, V. Ksenofontov, P. Adler, M. Nicklas, and C. Felser, Exchange-spring like magnetic behavior of the tetragonal Heusler compound  $\text{Mn}_2\text{FeGa}$  as a candidate for spin-transfer torque, *Appl. Phys. Lett.* **102**, 202402 (2013).
  - [8] S. V. Faleev, Y. Ferrante, J. Jeong, M. G. Samant, B. Jones, and S. S. Parkin, Heusler compounds with perpendicular magnetic anisotropy and large tunneling magnetoresistance, *Phys. Rev. Mater.* **1**, 024402 (2017).
  - [9] A. Kundu and S. Ghosh, First principles study of the structural phase stability and magnetic order in various structural phases of  $\text{Mn}_2\text{FeGa}$ , *Intermetallics* **93**, 209 (2018).
  - [10] L. Berger, Emission of spin waves by a magnetic multilayer traversed by a current, *Phys. Rev. B* **54**, 9353 (1996).
  - [11] J. C. Slonczewski, Current-driven excitation of magnetic multilayers, *J. Magn. Magn. Mater.* **159**, L1 (1996).
  - [12] J. Winterlik, S. Chadov, A. Gupta, V. Alijani, T. Gasi, K. Filsinger, B. Balke, G. H. Fecher, C. A. Jenkins, F. Casper, J. Kübler, G.-D. Liu, L. Gao, S. S. P. Parkin, and C. Felser, Design scheme of new tetragonal Heusler compounds for spin-transfer torque applications and its experimental realization, *Adv. Mater.* **24**, 6283 (2012).
  - [13] E. Krén and G. Kádár, Neutron diffraction study of  $\text{Mn}_3\text{Ga}$ , *Solid State Commun.* **8**, 1653 (1970).
  - [14] B. Balke, G. H. Fecher, J. Winterlik, and C. Felser,  $\text{Mn}_3\text{Ga}$ , a compensated ferrimagnet with high curie temperature and low magnetic moment for spin torque transfer applications, *Appl. Phys. Lett.* **90**, 152504 (2007).
  - [15] H. Kurt, K. Rode, M. Venkatesan, P. Stamenov, and J. M. D. Coey, High spin polarization in epitaxial films of ferrimagnetic  $\text{Mn}_3\text{Ga}$ , *Phys. Rev. B* **83**, 020405 (2011).
  - [16] R. Sahoo, L. Wollmann, S. Selle, T. Höche, B. Ernst, A. Kalache, C. Shekhar, N. Kumar, S. Chadov, C. Felser, S. S. P. Parkin, and A. K. Nayak, Compensated ferrimagnetic tetragonal Heusler thin films for antiferromagnetic spintronics, *Adv. Mater.* **28**, 8499 (2016).

- [17] C. Felser, V. Alijani, J. Winterlik, S. Chadov, and A. K. Nayak, Tetragonal Heusler compounds for spintronics, *IEEE Trans. Magn.* **49**, 682 (2013).
- [18] A. K. Nayak, M. Nicklas, S. Chadov, P. Khuntia, C. Shekhar, A. Kalache, M. Baenitz, Y. Skourski, V. K. Guduru, A. Puri, U. Zeitler, J. M. D. Coey, and C. Felser, Design of compensated ferrimagnetic Heusler alloys for giant tunable exchange bias, *Nat. Mater.* **14**, 679 (2015).
- [19] G. Kresse and J. Hafner, *Ab initio* molecular dynamics for liquid metals, *Phys. Rev. B* **47**, 558 (1993).
- [20] G. Kresse and J. Furthmüller, Efficient iterative schemes for *ab initio* total-energy calculations using a plane-wave basis set, *Phys. Rev. B* **54**, 11169 (1996).
- [21] P. E. Blöchl, Projector augmented-wave method, *Phys. Rev. B* **50**, 17953 (1994).
- [22] J. P. Perdew, J. A. Chevary, S. H. Vosko, K. A. Jackson, M. R. Pederson, D. J. Singh, and F. Fiolhais, Atom, molecules, solids, and surface: Applications of the generalized gradient approximation for exchange and correlation, *Phys. Rev. B* **46**, 6671 (1992).
- [23] J. P. Perdew, K. Burke, and M. Ernzerhof, Generalized gradient approximation made simple, *Phys. Rev. Lett.* **77**, 3865 (1996).
- [24] A. I. Liechtenstein, M. Katsnelson, V. Antropov, and V. Gubanov, Local spin density functional approach to the theory of exchange interactions in ferromagnetic metals and alloys, *J. Magn. Magn. Mater.* **67**, 65 (1987).
- [25] T. Ozaki, Variationally optimized atomic orbitals for large-scale electronic structures, *Phys. Rev. B* **67**, 155108 (2003).
- [26] H. Yoon, T. J. Kim, J.-H. Sim, S. W. Jang, T. Ozaki, and M. J. Han, Reliability and applicability of magnetic-force linear response theory: Numerical parameters, predictability, and orbital resolution, *Phys. Rev. B* **97**, 125132 (2018).
- [27] H. Yoon, T. J. Kim, J.-H. Sim, and M. J. Han, Jx: An open-source software for calculating magnetic interactions based on magnetic force theory, *Comput. Phys. Commun.* **247**, 106927 (2020).
- [28] M. J. Han, T. Ozaki, and J. Yu, Electronic structure, magnetic interactions, and the role of ligands in  $Mn_n$  ( $n=4, 12$ ) single-molecule magnets, *Phys. Rev. B* **70**, 184421 (2004).
- [29] See Supplemental Material at <http://link.aps.org/xxx> for comparison tetragonal and cubic phases for Mn (II) sites.  $\Delta E = E_T - E_C$  is plotted in Fig. S2 as function of Co concentration ( $x$ ).
- [30] W. S. Yun, G.-B. Cha, I. G. Kim, S. H. Rhim, and S. C. Hong, Strong perpendicular magnetocrystalline anisotropy of bulk and the (001) surface of  $D0_{22}$   $Mn_3Ga$ : a density functional study, *J. Phys.: Condens. Mater.* **24**, 416003 (2012).
- [31] See Supplemental Material at <http://link.aps.org/xxx> for magnetic moments using GGA+U calculations. The validity of applying on-site Coulomb interaction to  $Mn_3Ga$  is not justified yet. However, two cases are considered: (i)  $U$  for all magnetic atoms and (ii) only for Co atom, with  $U = 0 \sim 3$  eV. When  $U = 2$  eV on Co only, Co moment becomes  $-1.14 \mu_B$  while other  $U$  values Co magnetic moments are considerably smaller than the bulk value.
- [32] See Supplemental Material at <http://link.aps.org/xxx> for PDOS and magnetic moment of Ga atom. Ga moments are less than  $0.1 \mu_B$ .
- [33] L. Wollmann, G. H. Fecher, S. Chadov, and C. Felser, A scheme for spin-selective electron localization in  $Mn_3Ga$  Heusler material, *J. Phys. D: Appl. Phys.* **48**, 164004 (2015).
- [34] See Supplemental Material at <http://link.aps.org/xxx> for PDOS of Mn(I), Mn(II), and Co for various  $x$  for both cubic and tetragonal phases.